Sulfidation of Magnetite Nanoparticles - Following the Polysulfide Pathway

Georg Bendt,[a] Sascha Saddeler[a] and Stephan Schulz*[a]

Dedicated to Prof. Wolfgang Bensch on the occasion of his 65th birthday.

Abstract: The *in-situ* sulfidation of sub-10 nm sized Fe_3O_4 and partial-substituted $Co_xFe_{3-x}O_4$ (x = 0.25 - 0.75) nanoparticles by hot-injection of sulfur dissolved in oleylamine (OA) is strongly time- and temperature dependent. Fe_3O_4 nanoparticles are completely converted within 5 minutes into Fe_3S_4 nanoparticles under preservation of the spinel structure at 250 °C, whereas higher reaction temperatures and prolonged reaction times resulted in additional sulfur uptake and formation of pyrite FeS_2 nanoparticles. The formation of the cubic $(Co,Fe)S_2$ phase was observed in sulfidation reactions of $Co_xFe_{3-x}O_4$, even with low Co substitution levels (x = 0.25). The chemical composition, morphology and phase purity of the resulting nanoparticles were investigated by EDX, XRD, TEM and XPS.

Introduction

Magnetite Fe_3O_4 is known since ancient times and widely used as iron source. In contrast, the sulfur analogue Fe_3S_4 was firstly found 1964 in California.[1] Fe_3O_4 and Fe_3S_4 both crystallize in the cubic inverse spinel-type structure, but the lattice parameter of Fe_3S_4 (a = 9.876 Å) is 17 % larger compared to Fe_3O_4. Both materials show ferrimagnetic behavior and are typically described as semimetals, but theoretical and experimental studies recently demonstrated, that Fe_3S_4 rather behaves like a metal due to its covalent bonding character.[2,3] Fe_3S_4 has potential applications as substitute for Fe_3O_4, e.g. as anode material for high performance lithium-ion batteries,[4] in memory devices and in spintronics.[5,6] Another application of Fe_3S_4 nanoparticles is in the so-called hypothermal therapy, an experimental treatment of cancer based on the uptake of magnetic particles into cancer cells and their heating by an external magnetic field, which leads to the death of these cells.[7]

Unfortunately, the synthesis of high quality, phase-pure Fe_3S_4 material is challenging since the iron-sulfur system contains a large variety of different iron sulfides including $Fe_{1-x}S$ (pyrrhotite), FeS (trollite) $Fe_{1+x}S$ (mackinawite) and FeS_2 (pyrite and marcasite). In addition, the metastable nature of Fe_3S_4 favors its decomposition into $Fe_{1-x}S$ or FeS_2 upon thermal treatment. Despite these difficulties, several synthesis strategies for Fe_3S_4 were reported including the decomposition of *single source precursors* $Fe(Ddtc)_3$ in organic solvents[8,9] and in ionic liquids[10] at low reaction temperatures as well as in hydrothermal synthesis, respectively.[11-14] Very recently, the reaction pathways of iron-sulfide mineral formation under various conditions was studied by *in situ* X-ray diffraction.[15]

Direct sulfidation of metal oxides is a well established method for the synthesis of the corresponding metal sulfides. Cheng et al. established sulfidation reactions for the conversion of rocksalt-type CoO, FeO and MnO nanoparticles into the corresponding $Co_{1-x}S$, $Fe_{1-x}S$ and α-MnS particles,[16] while Ma et al. reported the formation of different copper sulfides by reacting CuO nanoparticles in aqueous solution with Na_2S.[17] Recently, Beal et al. synthesized small Fe_3S_4 nanoparticles (6.5 nm) by thermal decomposition of $Fe(acac)_2$ in hexadecylamine in combination with the hot-injection of elemental sulfur at 300 °C,[18] while magnetite (Fe_3O_4) nanoparticles were obtained in the absence of sulfur. In contrast, Fe_3S_4 nanosheets were obtained using the same procedure in oleylamine at 200 °C, whereas $Fe_{1-x}S$ nanoparticles were formed at 300 °C,[19] clearly demonstrating that the formation of Fe_3S_4 nanoparticles strongly depends on reaction time and reaction temperature. In addition, Fe_3S_4 thin films were deposited by *aerosol-assisted chemical vapor deposition* (AACVD) using heterocyclic dithiocarbamato-iron(III) complexes as single source precursor[20] as well as by DC magnetron sputtering.[21]

We herein report on the *in-situ* sulfidation of magnetite Fe_3O_4 nanoparticles, which allows the gram-scale synthesis of crystalline thiospinel Fe_3S_4 particles at 250 °C. In contrast, sulfidation of cobalt ferrite $Co_xFe_{3-x}O_4$ (x = 0.25 - 0.75) yields the cubic $(Co,Fe)S_2$ phase.

Results and Discussion

The thermal decomposition of metal acetylacetonates $M(acac)_x$ is well-established for the synthesis of metal oxide nanoparticles. $Fe(acac)_3$ is widely used as precursor for the synthesis of Fe_3O_4 nanoparticles, whose size and morphology strongly depends on the solvent, the solvent to precursor ratio, the specific capping agent and the reaction temperature.[22-25] We therefore initially investigated the thermal decomposition of $Fe(acac)_3$ in oleylamine (OA), which simultaneously serves as high-boiling solvent and as capping agent. The reaction time was kept constant for 45 minutes to ensure the complete consumption of the precursor, whereas the reaction temperature was varied from 200 over 250 to finally 300 °C in order to reveal its influence on the resulting particle size. The resulting particles were precipitated by addition of ethanol, isolated by

[a] Dr. G. Bendt, M. Sc. S. Saddeler, Prof. Dr. S. Schulz
Faculty of Chemistry and Center for NanoIntegration (CENIDE), University of Duisburg-Essen, Universitätsstr. 5-7, S07 S03 C30, D-45117 Essen, Germany
Fax: (+) 201-183 3830; E-mail: stephan.schulz@uni-due.de
https://www.uni-due.de/ak_schulz/index_en.php

Supporting information for this article is given via a link at the end of the document.

centrifugation and purified by several washing steps using a 1:1 mixture of ethanol and chloroform mixture.

XRD patterns of the resulting materials show broad Bragg reflections due to the nanocrystalline nature of the particles (Fig. 1A). The peaks can be indexed on the cubic spinel structure of Fe_3O_4 (ICSD 19-0629).

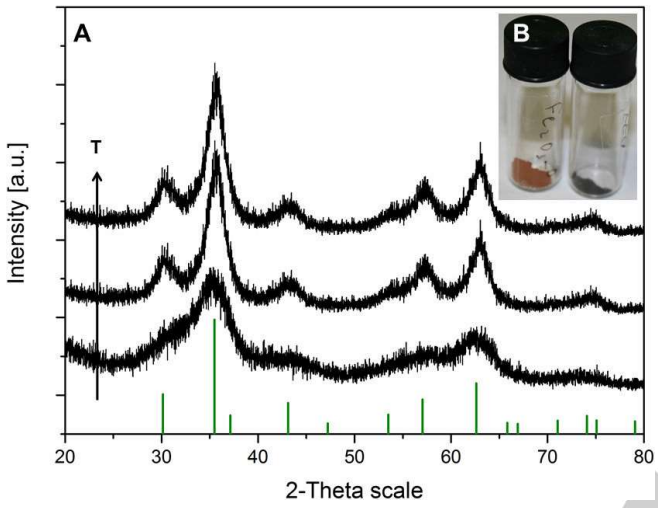

Figure 1: PXRDs of Fe_3O_4 nanoparticles as obtained by thermal decomposition of $Fe(acac)_3$ in OA at 200 °C, 250 °C and 300 °C and reference (green: PDF 19-0629 (Fe_3O_4)) Inset: Photography of iron oxide nanoparticles prepared at 200 °C (left) and 250 °C (right).

With increasing reaction temperature, the reflections become significantly sharper, indicating the growth of larger particles. Based on the XRD pattern, the average particle sizes were determined by Rietveld refinement to 5 nm (200 °C), 7 nm (250 °C) and 9 nm (300 °C), respectively. While the XRD patterns suggest the formation of phase-pure Fe_3O_4 nanoparticles, the red-brownish color of the sample (Fig. 1B) prepared at 200 °C indicates the presence of maghemite γ-Fe_2O_3 as a second phase. Both iron oxide phases crystallize in the cubic spinel lattice, but Fe_3O_4 is an inverse spinel, in which half of the octahedral positions are occupied by Fe^{2+} cations, whereas the remaining octahedral and the tetrahedral positions are filled with Fe^{3+} cations. In contrast, γ-Fe_2O_3 is an inverse spinel containing only Fe^{3+} cations, which exclusively occupy the tetrahedral positions, whereas two vacancies are formed on the octahedral positions. The comparable crystal structures of γ-Fe_2O_3 and Fe_3O_4 leads to similar XRD pattern, in which only the 311 reflection is slightly shifted to higher diffraction angles for γ-Fe_2O_3 compared to Fe_3O_4. Therefore, the exact phase analysis for nanosized materials and in particular for phase mixtures is hampered due the broad reflections.

Fig. 2A displays a typical TEM image of the magnetite sample prepared at 250 °C, showing spherical particles with diameters of roughly 7 nm with a narrow size distribution. The SAED pattern obtained from an array of particles (Fig 2B) is in good agreement with the literature data and clearly shows the formation of phase-pure Fe_3O_4, as was proven by comparison with calculated ED-pattern using data from (ICSD 19-0629). The particle size histogram is given in Fig 2C.

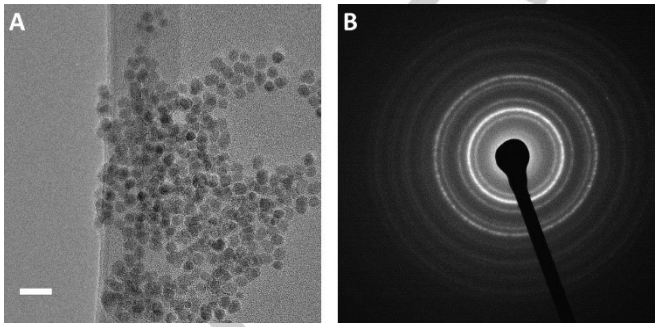

Figure 2: TEM images of the Fe_3O_4 nanoparticles prepared at 250 °C, scale bar: 20 nm (**A**), SAED pattern (**B**).

Effect of the reaction temperature on the sulfidation of 7 nm Fe_3O_4 particles

The effect of the reaction temperature on the sulfidation reaction was studied using 7 nm Fe_3O_4 nanoparticles, which were *in situ* prepared at 250 °C.[26] After 45 min, a freshly prepared solution of sulfur (S_8) in oleylamine OA was injected into the hot reaction mixture. The synthetic approach is similar to the one described by Beal et al.[18] Immediately after the injection, the dark brown dispersion turned black. The S_8/OA mixture is widely used in nanoparticles synthesis and contains alkyl ammonium polysulfides, which generates H_2S at higher temperatures.[27] The *in-situ* sulfidation reaction was performed between 200 and 300 °C in order to investigate the impact of the reaction temperature (Fig. 3). The size stability of the starting Fe_3O_4 nanoparticles in solution in this temperature regime was before proven in an independent study, in which isolated Fe_3O_4 nanoparticles (5, 7 and 9 nm) were heated for 3 h at the desired temperature. Ostwald ripening of the starting Fe_3O_4 nanoparticles was never observed within these short reaction times. After 15 minutes, the reaction mixture was cooled down and the resulting material was precipitated by addition of ethanol, isolated by centrifugation and purified by several washing steps with an ethanol/chloroform mixture (1:1).

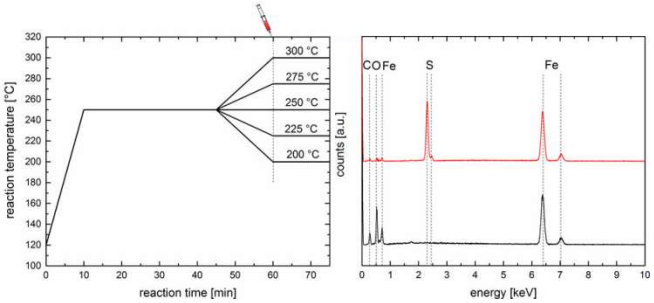

Figure 3: Temperature profile for the sulfidation of 5 nm Fe_3O_4 nanoparticles, EDX spectra of isolated starting Fe_3O_4 nanoparticles (black) and of the resulting nanoparticles after sulfidation reaction at 250 °C (red).

According to EDX studies, the sulfur content steadily increases with increasing reaction temperature (Table 1). The Bragg

reflections in the diffractograms of samples **III-V** correspond to Fe_3S_4 (**III**) and a mixture of cubic FeS_2 (pyrite) and Fe_3S_4 (**IV**, **V**), again showing strong broadening due the nanosized nature of the materials, whereas the sample **I** and **II** are amorphous (Fig. 4). No reflections indicating the presence of the Fe_3O_4 starting material are visible. The formation of phase pure Fe_3S_4 and the absence of any Fe_3O_4 starting material in sample **III** was also proven by Raman spectroscopy. The Raman spectrum (Fig. S5) of the 7 nm-sized Fe_3O_4 nanoparticles prepared at 250 °C and the resulting Fe_3S_4 particles prepared at 250 °C (sample **III**) only showed absorption bands in the expected region at 687 cm^{-1} (Fe_3O_4) and 354 cm^{-1} (Fe_3S_4), which is in good agreement with the literature value for the T_{2g1} mode corresponding to the asymmetric bending of the Fe-S bond in Fe_3S_4 (350 cm^{-1}).[13]

Table 1. Phase composition and particle size of iron sulfides obtained at different reaction temperatures.

Sample	T [°C]	Phase[a]	Size[a] [nm]	Fe [at%]	S [at%]
I	200	amorphous	-	63.8	36.2
II	225	amorphous	-	56.0	44.0
III	250	Fe_3S_4	5.7	54.4	45.6
IV	275	Fe_3S_4 FeS_2	6.2 10	47.1	52.9
V	300	Fe_3S_4 FeS_2	6.3 15.4	41.1	58.9

[a] The particle size of the nanoparticles was determined from powder diffractograms by using the Debye-Scherrer equation.

To further determine the nature of the amorphous material obtained at 200 °C (sample **I**), the solid was washed with OA at ambient temperature to remove additional sulfur, suspended in OA and annealed at 300 °C for 1 h, resulting in the formation of a black suspension. The resulting material was isolated by centrifugation and purified by repeated washing with $CHCl_3$.

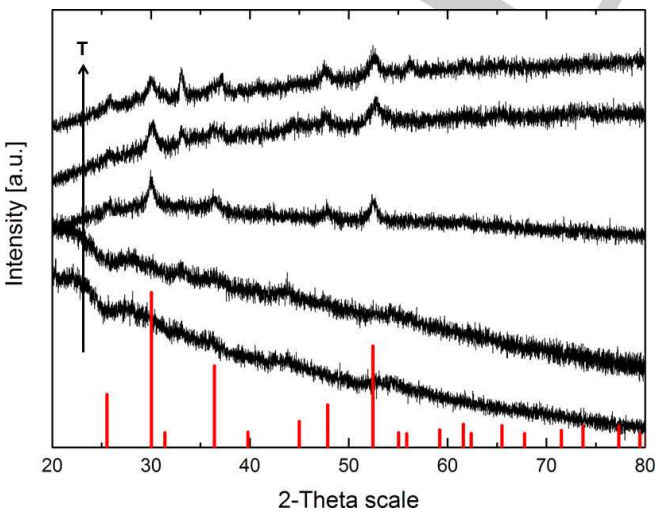

Figure 4: XRD pattern of the reaction products of the sulfidation of 7 nm Fe_3O_4 at different temperatures and reference (red PDF 01-089-2000 Fe_3S_4).

The XRD pattern (Fig. S3) shows sharp reflexes due to the presence of large, non-stoichiometric $Fe_{1-x}S$ (pyrrhotite) particles. Elemental analysis (EDX) proved the Fe:S ratio close to one. According to these results, the original amorphous material is not stable under these specific conditions. The phase-pure Fe_3S_4 sample obtained at 250 °C (**III**) was investigated by XPS (Fig. 5) after storage under air for 4 weeks. The emission of the Fe $2p_{3/2}$ (**5A**) spectrum can be best fitted on the basis of the interpretation of Han et al. as a complex mixture of Fe^{2+}-S and Fe^{3+}-S (peaks in the range 706-710 eV) as well as Fe^{3+}-O (peaks in the range 710-714 eV).[29] The S $2p_{3/2}$ spectrum (**5C**) shows a comparable complexity and can be separated into two parts. Peaks at low binding energy (160-165 eV) point to the presence of mono-, di- and polysulfides, while peaks at higher binding energy correspond to elemental sulfur, sulfite and sulfate. The O 1s (**5B**) spectrum shows one singlet at 530 eV (O^{2-}) and a second singlet shifted to higher binding energy caused by hydroxyl and sulfate ions on the particles surface.

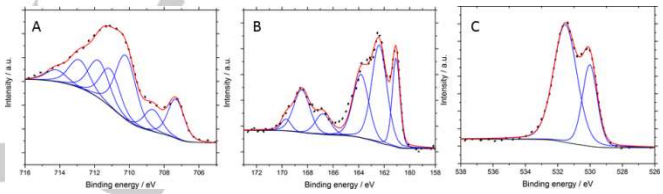

Figure 5: XPS core level spectra of Fe_3S_4 obtained at 250 °C; Fe $2p_{3/2}$ (**A**), O 1s (**B**) and S $2p_{3/2}$ (**C**).

The particle morphology and size of the phase-pure Fe_3S_4 nanoparticles obtained at 250 °C was further analyzed by TEM (Fig. 6A), showing a broad particles size distribution in the range of 20 nm. In contrast to the starting Fe_3O_4 nanoparticles, which showed a uniform spherical morphology, the morphology of the sulfidation product is rather non-uniform including the presence of distorted triangular and hexagonal plates.

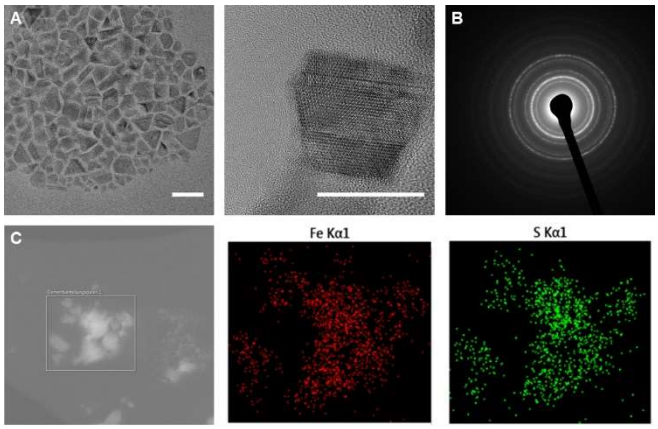

Figure 6: TEM pictures, scale bar: 50 and 20 nm **(A),** SAED pattern **(B)** and elemental mapping **(C)** of Fe_3S_4 nanoparticles prepared at 250 °C.

The corresponding SAED pattern (Fig. 6B), which can be indexed on the spinel-type crystal structure of Fe_3S_4 (Fig. S4), consist of a mixture of diffuse diffraction rings and distinct spots,

pointing to the presence of larger crystals compared to the starting Fe_3O_4 nanoparticles. EDX mapping (Fig. 6C) of large area including several different particle morphologies proves the uniform distribution of iron and sulfur within the nanoparticles. An enhanced oxygen concentration was not observed, indicating the complete sulfidation of the Fe_3O_4 nanoparticles.

Effect of the reaction time on the sulfidation reaction of 7 nm Fe_3O_4 particles

The sulfidation reaction of Fe_3O_4 nanoparticles at 250 °C was almost completed after 15 minutes as demonstrated before. To get further insights into the conversion process, the reaction time was varied between 5 and 30 minutes without changing any other reaction parameter. The chemical composition of the resulting materials was determined by EDX, showing an increasing sulfur content with the reaction time (Table 2).

Table 2. Phase composition and particle size of iron sulfides after different sulfidation times.

Sample	time [min]	Phase[a]	Size[a] [nm]	Fe [at%]	S [at%]
VI	5	Fe_3S_4	5	53.1	46.9
VII	10	Fe_3S_4	5.7	54.4	45.6
VIII	30	Fe_3S_4 FeS_2	6.1 15.7	44.0	56.0

[a] The particle size of the resulting nanoparticles was determined from powder diffractograms by using the Debye-Scherrer equation.

The starting material was completely consumed even after the short reaction time of five minutes as was demonstrated by X-ray diffraction. The XRD pattern of the resulting material (Fig. 7) only shows the presence of phase pure Fe_3S_4 (**VI**), whereas no reflections due to crystalline Fe_3O_4 were observed.

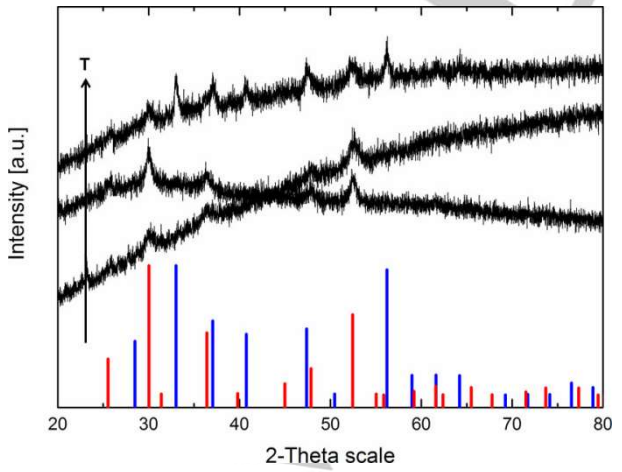

Figure 7: XRD pattern of the reaction products of the sulfidation of 7 nm-sized Fe_3O_4 nanoparticles after 5, 15 and 30 minutes and reference (red: Fe_3S_4, PDF: 01-089-2000; blue: FeS_2, PDF: 6-710).

Extension of the reaction time up to 15 minutes only resulted in sharper reflections of as-formed Fe_3S_4, proving the formation of larger particles (**VII**). When the reaction time was extended to 30 minutes, the spinel phase (Fe_3S_4) is converted into the cubic phase (FeS_2), indicating the uptake of additional sulfur under these sulfur-rich reaction conditions.

Effect of the sulfur concentration

The previous sulfidation reaction of Fe_3O_4 nanoparticles were performed with 4.0 mmol of sulfur and 1.0 mmol of $Fe(acac)_3$. To investigate the role of the amount of sulfur in the reaction, 7 nm sized *in situ* formed Fe_3O_4 nanoparticles were reacted with different amounts of sulfur (1.33, 2.0, 4.0 and 6.0 mmol) at 250 °C (Table S3).[26] The reaction with a stochiometric amount of sulfur (1.33 mmol) yielded particles showing an very low sulfur to iron ratio of 0.14:1, which is far below the expected value of 1.33:1 for Fe_3S_4 in case of a stoichiometric reaction. The XRD pattern of the resulting material only shows reflections due to the formation of crystalline Fe_3O_4 (Fig. S4) without any other crystalline phases. In contrast, reactions with larger amounts of sulfur yielded materials with higher sulfur to iron ratios of 0.34:1 (2.0 mmol), 0.84:1 (4.0 mmol) and 0.98:1 (6.0 mmol), respectively. Even with the highest sulfur concentration, the reaction failed to give a molar ratio of 1.33:1 as is expected for pure for Fe_3S_4. The formation of sulfur-deficient particles might be caused by the fact that the sulfidation reaction proceeds via diffusion of sulfur atoms into the Fe_3O_4 nanoparticles and subsequent substitution of the oxygen atoms. Therefore, the substitution of the oxygen atoms at the surface of the nanoparticles should be rather fast, whereas the diffusion rate is expected to slow down towards the center of the nanoparticles. Therefore, the sulfidation reaction is not complete, leading to sulfur-deficient materials. To complete the reaction, longer reaction times would be necessary, but this is hampered by the metastable character of Fe_3S_4. Therefore, sulfur-rich FeS_2 is typically formed at elevated reaction times and temperatures.

TEM images of the sulfurized particles as obtained with 1.33 mmol of sulfur show the formation of spherical particles comparable to the starting material (Fig. 8). These studies also clearly demonstrate, that the starting Fe_3O_4 nanoparticles don't change their size under the reaction conditions.

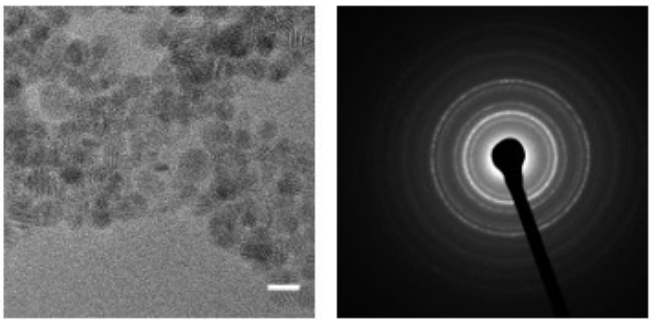

Figure 8: TEM image of the nanoparticles obtained from the sulfidation reaction of 6 nm Fe_3O_4 with 1.33 mmol of sulfur, scale bar: 10 nm (left) and the corresponding SAED pattern (right).

The SAED pattern is identical to the X-ray diffractogram of the Fe_3O_4 starting material. According to these findings, we assume that the small amount of sulfur (Fe:S ratio = 0.14:1) is located as thin, most likely amorphous layer on the Fe_3O_4 nanoparticles surface. Use of a higher amount of sulfur yield nanoparticles with a higher sulfidation degree as proven by EDX, whereas no changes in the XRD pattern were visible. The TEM image of the resulting nanoparticles shows no significant changes compared to the starting Fe_3O_4 nanoparticles. The formation of a biphasic system, consisting of crystalline iron oxides and iron sulfides, was not detected in any case and can therefore be excluded. Instead, the formation of particles, which contain a crystalline Fe_3O_4 core and an amorphous iron sulfide shell is likely.

Effect of Fe_3O_4 particle size

The temperature- and time dependent sulfidation reaction of 7 nm-sized Fe_3O_4 nanoparticles demonstrated their high reactivity towards the sulfur/OA mixture and the fast formation of the crystalline thiospinel phase Fe_3S_4 within five minutes at 250 °C, whereas the similarly fast formation of amorphous $Fe_{1-x}S$ was observed at lower reaction temperatures. With the goal to decelerate the sulfidation reaction and to resolve the process into smaller steps, the sulfidation reaction was repeated at 250 °C with magnetite particles of different sizes, which were prepared by controlling the reaction temperature during the thermal decomposition of the $Fe(acac)_3$ precursor. Assuming the occurrence of diffusion-controlled processes, the sulfidation-time is expected to increase with increasing size of the Fe_3O_4 nanoparticles, while the size of the resulting particles should be comparable to that of the starting particles.

Fig. 9A shows the temperature profile of the whole reaction process. 5, 7 and 9 nm Fe_3O_4 nanoparticles were first synthesized at 200, 250 and 300 °C, respectively. After the iron acetylacetonate precursor (1 mmol) was fully consumed (45 min), the reaction temperature was adjusted to 250 °C and the sulfur (4 mmol)/OA mixture was injected. The sulfidation reaction was performed for 15 minutes and the resulting nanomaterials precipitated by addition of ethanol and then isolated by filtration.

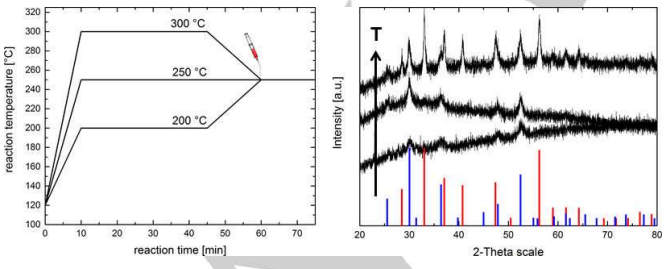

Figure 9: Temperature profile for the sulfidation of Fe_3O_4 nanoparticles with different particle sizes. XRD pattern of the reaction products of the sulfidation of 5, 7 and 9 nm Fe_3O_4 after 15 minutes and reference (blue: Fe_3S_4; red: FeS_2)

The XRD patterns of the resulting materials are displayed in Fig. 9B. As was expected, a linear relationship between the size of the starting Fe_3O_4 nanoparticles and the size of the resulting phase pure Fe_3S_4 nanoparticles as determined by using the Debye-Scherrer equation was observed. Surprisingly, the sulfidation of 9 nm sized Fe_3O_4 nanoparticles yielded FeS_2 as major phase. Each reaction was repeated for five times, always yielding Fe_3S_4 nanoparticles (5, 7 nm starting Fe_3O_4) and FeS_2 nanoparticles (9 nm starting Fe_3O_4), respectively.

The fast formation of phase-pure Fe_3S_4 nanoparticles in the sulfidation experiments using small 5 and 7 nm-sized Fe_3O_4 nanoparticles most likely results from the short diffusion pathway. In addition, the different thermal history of the size selective synthesis of magnetite particles may have a beneficial effect. With decreasing synthesis temperature of the Fe_3O_4 nanoparticles (200 °C: 5 nm; 250 °C: 7 nm; 300 °C: 9 nm), the formation of crystal structure (lattice) defects and of strain, which are both beneficial for the diffusion of sulfur and therefore the formation of Fe_3S_4, becomes more probable. In addition, the presence of γ-Fe_2O_3 in the Fe_3O_4 starting material as was observed in the 5 nm-sized Fe_3O_4 nanoparticles might play an important role, since vacancies in the maghemite structure positively affect the diffusivity of the material as was shown before.[30] However, these effects do not explain the formation of FeS_2 nanoparticles in case of the 9 nm-sized Fe_3O_4 particles.

Effect of metal substitution $Co_xFe_{3-x}O_4$ (x = 0.25 - 0.75)

Substitution of Fe^{2+} in Fe_3O_4 by bivalent cations, i.e. Co^{2+} and Ni^{2+}, yields a wide range of solid solutions of MFe_2O_4 spinels (M = Co, Ni), which are also found in nature as minerals. In contrast, the corresponding thiospinels show a more complex behavior. The complete solid solution series between greigite Fe_3S_4 and polydymite Ni_3S_4 is known as naturally occurring mineral violarite $Ni_xFe_{3-x}S_4$,[31] whereas negligible solid-solutions exists between linnaeite Co_3S_4 and Fe_3S_4.[32] We therefore studied the sulfidation of the substituted mixed-metal spinels $Co_xFe_{3-x}O_4$ as a possible synthetic route for the preparation of the corresponding thiospinels.

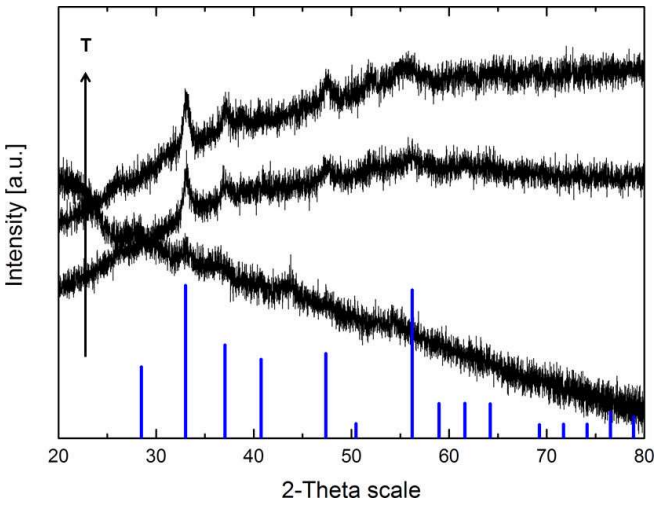

Figure 10: XRD pattern of the reaction products of the sulfidation of $Co_xFe_{3-x}O_4$ (x = 0.25, 0.5, and 0.75) and reference (blue FeS_2).

$Co_xFe_{3-x}O_4$ (x = 0.25 - 0.75) nanoparticles synthesized at 250 °C were used as precursor for the sulfidation reaction by a procedure recently reported by us.[33] The elemental composition of the different cobalt iron oxides were determined by EDX. Fig. 10 displays the XRD pattern of the isolated particles as obtained with $Co_xFe_{3-x}O_4$ (x = 0.25 - 0.75) nanoparticles as starting material, showing the formation of $(Co,Fe)S_2$ particles (cubic phase) even for low cobalt concentrations. The formation of a crystalline mixed-metal spinel can be excluded. We are currently investigating sulfidation reactions of other mixed-metal spinels to further evaluate the applicability of the described reaction process for the synthesis of mixed-metal thiospinels.

Conclusions

Sulfidation reactions of sub-10 nm sized Fe_3O_4 nanoparticles with elemental sulfur in solutions of oleylamine were investigated in detail. A strong effect of the reaction temperature and time, the sulfur concentration, and the particle size of the starting Fe_3O_4 nanoparticles on the sulfidation degree and the resulting structural phase and size of sulfur-containing particles were identified. The sulfidation reaction mimics the “polysulfide pathway”, a well-known process for the transformation of sulfur-poor into sulfur-rich iron sulfides in nature. At low reaction temperatures, the fast formation of an amorphous iron sulfide occurs, which crystallizes during *ex-situ* annealing at 250 °C as $Fe_{1-x}S$. A higher reaction temperature of 250 °C yields crystalline, phase-pure thiospinel Fe_3S_4 particles, whereas the formation of FeS_2 starts at higher reaction temperature (275 °C). FeS_2 becomes the dominate phase at 300 °C. Determination of the magnetic properties of the starting Fe_3O_4 nanoparticles as well as the sulfidation products Fe_3S_4 and FeS_2 as obtained under different reaction conditions are of particular interest. These studies are currently performed, and the results will be presented in the near future. Moreover, more detailed studies on the reaction mechanism of the metal sulfide formation process are currently performed in order to gain further insights and a profound mechanistical understanding of the synthesis of binary and ternary iron sulfides.

Experimental Section

Materials. The starting metal acetylacetonates $Co(acac)_2$ and $Fe(acac)_3$ were purchased from Sigma-Aldrich and used without further purification. Elemental sulfur (99.999 %, 100 mesh) was obtained from ABCR. Oleylamine (80-90 %) was obtained from Acros organics and was degassed prior to use.

Sulfidation reactions at different reaction times

353 mg $Fe(acac)_3$ (1.00 mmol) was suspended in 6 g of oleylamine and heated to 120 °C for 60 min to remove any volatile impurities and moisture, resulting in a clear red solution. The temperature was then raised to the final reaction temperature (200, 225, 250, 275 and 300 °C) and a solution of 128 mg sulfur (4.0 mmol) in 2 mL of oleylamine was injected into the hot Fe_3O_4 dispersion, which turned immediately dark black. The reaction mixture was stirred for additional 15 minutes at the desired temperature and then cooled to ambient temperature. The resulting nanoparticles were precipitated by addition of 10 mL of ethanol, isolated by centrifugation, purified by repeated washing (2-3 times) with a mixture of ethanol and chloroform and finally dried in vacuum.

Structural Characterization

XRD. Powder X-ray diffractograms of the resulting nanoparticles were recorded at ambient temperature (25 ± 2 °C) using a Bruker D8 Advance powder diffractometer in Bragg–Brentano mode with Cu Kα radiation (λ = 1.5418 Å, 40 kV and 40 mA). The powder samples were investigated in the range of 20 to 80° 2 θ with a step size of 0.01° and a counting time of 0.3 s.

SEM and EDX. Scanning electron microscopy studies were performed with a Jeol JSM 6510 equipped with an energy-dispersive X-ray spectroscopy (EDX) device (Bruker Quantax 400).

TEM. Transmission electron microscopy studies were performed using a JEOL 2200FS with an acceleration voltage of 200 kV.

FT-IR spectroscopy. IR spectra were recorded with a Bruker Alpha FT-IR spectrometer equipped with a single-reflection ATR sampling module.

XPS. XPS studies were performed using a Versaprobe IITM (Ulvac-Phi) with monochromatic Al Kα light at 1486.6 eV photon energy. The emission angle between analyzer and sample is 45°. The Cu 2p signal at 932.67 eV binding energy of a sputter cleaned Cu foil was used as the binding energy reference. The foil and the powder were put onto insulating double-sided tape and charging effects were compensated using a dual-beam neutralizing approach using electrons and slow-moving argon ions.

Raman spectroscopy. Raman spectra were measured using a Renishaw InVia Raman microscope with a laser wave length of 633 nm.

Acknowledgements

Financial support by the University of Duisburg-Essen is acknowledged. TEM, XPS and Raman measurements were performed at the Interdisciplinary Center for Analytics on the Nanoscale (ICAN) in Duisburg.

Keywords: Iron • Magnetide • Nanoparticles • Spinel phases • Sulfur

[1] B. J. Skinner, R. C. Erd, F. S. Grimaldi, *Am. Mineral.* **1964**, *49*, 543–555.
[2] B. Zhang, G. A. De Wijs, R. A. De Groot, *Phys. Rev. B* **2012**, *86*, 020406.

[3] G. Li, B. Zhang, F. Yu, A. A. Novakova, M. S. Krivenkov, T. Y. Kiseleva, L. Chang, J. Rao, A. O. Polyakov, G. R. Blake, R. A. de Groot, T. T. M. Palstra, *Chem. Mater.* **2014**, *26*, 5821–5829.

[4] a) J. Zheng, Y. Cao, C. Cheng, C. Chen, R. Yan, H. Huai, Q. Dong, M. Zheng, C. Wang, *J. Mater. Chem. A* **2014**, *2*, 19882–19888; b) Q.-T. Xu, J.-C. Li, H.-G. Xue, S.-P. Guo, *J. Power Sources* **2018** *379*, 41–52; c) Q. Zhang, J. P. Mwizerwa, H. Wan, L. Cai, X. Xu, X. Yao, *J. Mater. Chem. A* **2017**, *5*, 23919–23925.

[5] M. Wu, J. S. Tse, Y. Pan, *Sci. Rep.* **2016**, *6*, 21637.

[6] J. Wang, S. Cao, W. Wu, G. Zhao, *Phys. Scr*. **2011**, *83*, 045702–7.

[7] a) Y. Chang, S. Savitha, S. Sadhasivam, C. Hsu, F. Lin, *J. Colloid Interface Sci.* **2011**, *363*, 314–319; b) L. Argueta-Figueroa, O. Martinéz-Alvarez, J. Sontos-Cruz, R. Garcia-Contreras, L. S. Acosta-Torres, J. de la Fuente-Hernández, M. C. Arenas-Arrocena, *Mater. Sci. Eng. C* **2017**, *76*, 1305–1315; D. Karponis, M. Azzawi, A. Seifalian, *Nanomedicine* **2016**, *11*, 2215–2230; d) K. Simeonidis, S. Liébana-Viñas, U. Wiedwald, Z. Ma, Z.-A. Li, M. Spasova, O. Patsia, E. Myrovali, A. Makridis, I. Tsiaoussis, G. Vourlias, M. Farle, *RSC Adv.* **2016**, *6*, 53107–53117.

[8] W. Han, M. Gao, *Cryst. Growth Des*. **2008**, *8*, 1023–1030.

[9] Y. Zhang, Y. Du, Q. Wang, *Cryst. Eng. Comm*. **2010**, *12*, 3658–3663.

[10] J. Ma, L. Chang, J. Lian, Z. Huang, X. Duan, X. Liu, *Chem. Comm*. **2010**, *46*, 5006–5008.

[11] F. Cao, W. Hu, L. Zhou, W. Shi, S. Song, Y. Lei, *Dalton Trans*. **2009**, *42*, 9246–9252.

[12] M. J. Dekkers, M. A. A. Schoonen, *Geophys. J. Int*. **1996**, *126*, 360–368.

[13] a) Lu, J., Tsai, C., *Nanoscale Res. Lett.* **2014**, *9*, 230–238, b) G. Li, B. Zhang, F. Yu, A. A. Novakova, M. S. Krivenkov, T. Y. Kiseleva, L. Chang, J. Rao, A. O. Polyakov, G. R. Blake, R. de Groot, T. T. M. Palstra, *Chem. Mater*. **2014**, *26*, 5821–5829.

[14] P. Li, C. Xia, Q. Zhang, Z. Guo, W. Cui, H. Bai, H. N. Alshareef, X.-X Zhang, *J. Appl. Phys*. **2015**, *117*, 223903.

[15] M.-Y. Lin, Y.-H. Chen, J.-J. Lee, H.-S. Sheu, Eur. J. Mineral. 2018, 30, 77–84.

[16] C.-J. Chen, R.-K. Chiang, *Dalton Trans*. **2011**, *40*, 880–885.

[17] R. Ma, J. Stegemeier, C. Levard, J. G. Dale, C. W. Noack, T. Yang, E. Brownjr, G. V Lowry, *Environ. Sci. Nano* **2014**, *1*, 347–357.

[18] J. H. L. Beal, S. Prabakar, N. Gaston, G. B. Teh, P. G. Etchegoin, G. Williams, R. D. Tilley, *Chem. Mater*. **2011**, *25*, 2514–2517.

[19] J. H. L. Beal, P. G. Etchegoin, R. D. Tilley, *J. Solid State Chem*. **2012**, *189*, 57–62.

[20] S. Mlowe, D. J. Lewis, M. A. Malik, J. Raftery, E. B. Mubofu, P. O. Brien, N. Revaprasadu, *Dalton Trans*. **2016**, *45*, 2647–2655.

[21] H. Lui, D. Chi, *J. Vac. Sci. Technol*. **2012**, *30*, 04D102.

[22] G. Gao, X. Liu, R. Shi, K. Zhou, Y. Shi, R. Ma, E. Takayama-Muromachi, G. Qiu, *Cryst. Growth Des*. **2010**, *10*, 2888–2894.

[23] J. Xie, S. Peng, N. Brower, N. Pourmand, S. X. Wang, S. Sun, *Pure Appl. Chem*. **2006**, *78*, 1003–1014.

[24] Z. Xu, C. Shen, Y. Hou, H. Gao, S. Sun, *Chem. Mater*. **2009**, *21*, 1778–1780.

[25] S. Sun, H. Zeng, D. B. Robinson, S. Raoux, P. M. Rice, S. X. Wang, G. Li, *J. Am. Chem. Soc.* **2004**, *126*, 273-279.

[26] Sulfidation reactions with isolated and re-dispersed Fe_3O_4 nanoparticles yielded the same reaction products as was obtained from *in-situ* sulfidation reactions, demonstrating that this reaction is independent from by-products of the initial thermolysis reaction.

[27] J. W. Thomson, K. Nagashima, P. M. Macdonald, G. A. Ozin, *J. Am. Chem. Soc*. **2011**, *133*, 5036–5041.

[28] S. Hunger, L. G. Benning, *Geochem. Trans*. **2007**, *8*, 1–20.

[29] W. Han, M. Gao, *Cryst. Growth Des*. **2008**, *8*, 1023–1030.

[30] C. Carbonin, A. D. Giusta, *Z. Krist. New Cryst. Struct.* **1991**, *194*, 111–119.

[31] D. J. Vaughan, J. R. Craig, *Am. Mineral*. **1985**, *70*, 1036–1043.

[32] D. J. Vaughan, R. G. Burns, V. M. Burns, *Geochim. Cosmochim. Acta* **1971**, *35*, 365–381.

[33] a) K. Chakrapani, G. Bendt, H. Hajiyani, I. Schwarzrock, T. Lunkenbein, S. Salamon, J. Landers, H. Wende, R. Schlögl, R. Pentcheva, M. Behrens, S. Schulz, *Chem. Cat. Chem.* **2017**, *9*, 2988–2995; b) K. Chakrapani, G. Bendt, H. Hajiyani, T. Lunkenbein, M. Greiner, L. Masliuk, S. Salamon, J. Landers, R. Schlögl, H. Wende, R. Pentcheva, S. Schulz, M. Behrens, *ACS Catalysis* **2018**, *8*, 1259–1267.

Entry for the Table of Contents

Layout 1:

FULL PAPER

Sulfidation of Fe_3O_4 nanoparticles with elemental sulfur in oleylamine occurs with preservation of the spinel-type structure and formation of Fe_3S_4. In contrast, sulfidation reactions of $Co_xFe_{3-x}O_4$ ($x < 0.5$) yielded cubic-phase $(Co,Fe)S_2$ particles.

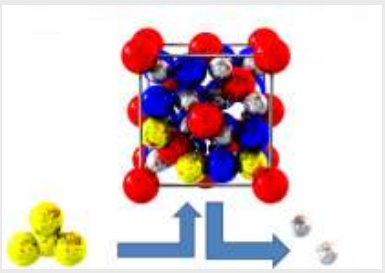

*Georg Bendt, Sascha Saddeler, Stephan Schulz**

Page No. – Page No.

Sulfidation of Magnetite Nanoparticles - Following the Polysulfide Pathway

Additional Author information for the electronic version of the article.

Stephan Schulz: orcid.org/0000-0003-2896-4488

DOI: 10.1002/ejic.201801075
URN: urn:nbn:de:hbz:464-20210127-134907-5

This is the peer reviewed version of the following article: Bendt, G., Saddeler, S., Schulz, S.: Sulfidation of Magnetite Nanoparticles - Following the Polysulfide Pathway. *Eur. J. Inorg. Chem.* 2019, 05, 602-608, which has been published in final form at: https://doi.org/10.1002/ejic.201801075